Time -Resolved SAXS Studies of Periodic Mesoporous Organosilicas in Anodic Alumina Membranes

John M. O' Callaghan[†], Nikolay Petkov[‡], Mark P. Copley[†], Donna C. Arnold[†], Michael A. Morris[†], Heinz Amenitsch[ϕ] and Justin D. Holmes[†,]*

[†]Materials and Supercritical Fluids Group, Department of Chemistry and the Tyndall National Institute, University College Cork, Cork, Ireland and the Centre for Research on Adaptive Nanostructures and Nanodevices (CRANN), Trinity College Dublin, Dublin 2, Ireland.

[‡]Electron Microscopy and Analysis Facility (EMAF), Tyndall National Institute, Lee Maltings, Prospect Row, Cork, Ireland

[ϕ]Institute for Biophysics and Nanosystems Research, Austrian Academy of Sciences Schmiedlstraße 6, 8042 Graz.

* To whom correspondence should be addressed: Tel: +353(0)21 4903608; Fax: +353 (0)21 4274097; E-mail: j.holmes@ucc.ie

Abstract

A method for producing oriented periodic mesoporous organosilica filaments within the confined channels of anodic alumina membranes is presented. Deposition of the mesoporous filaments were performed under a variety of conditions, which favoured the evaporation induced self-assembly of the mesoporous material. The experimental conditions examined included different drying rates, over a range of humidity values, and sol composition, *e.g.* varying the amount of the organosilica component. The deposition process was followed *in-situ* by time resolved small angle x-ray scattering which was essential for evaluating the formation mechanism of the mesophase structures. Through careful control of the deposition environment, the structure and orientation of the mesoporous filaments could readily be varied.

Keywords

Ordered mesoporous materials, periodic mesoporous silica, small angle x-ray scattering evaporation induced self assembly.

Introduction

Periodic mesoporous organosilicas (PMOs) are an attractive class of ordered mesoporous materials consisting of hybrid structural units, *i.e.* -[$_{1.5}$OSi-R-SiO$_{1.5}$]- (where R is a bridged group, such as -CH_2CH_2-, -CH=CH-, or phenyl) where the inorganic and organic moieties in the structure are covalently linked to each other [1-5]. PMO materials offer novel porous structures with different chemical characteristics to the traditional inorganic-based mesoporous materials. These materials combine the rigidity of the silica framework with the added functionality of the organic counterpart. The organo-silica functionality is generated during the initial synthesis of

the material by hydrolysis of an appropriate organo-silica precursor which results in the formation of a material with a repeating organic bridging unit [6]. PMOs have found use in a wide range of applications including catalysis [5], chromatography [7] and as high k dielectrics [8] as reviewed by Wight *et. al.* [9] and Hoffmann *et. al.* [10]. Thin films of PMO materials have also been prepared by the deposition of suitable gels onto substrates, for example Wu *et al.*[11] have reported the production of PMO thin films on silicon substrates. The formation of mesoporous materials within the confined architecture of a structured template, for example anodic alumina membranes (AAMs) [12, 13] provides a unique opportunity to spatially align the mesopores in a particular orientation due to the directional alignment of the pores within the template. Similar mesoporous silica filaments were reported by Huo *et al.* in 1997 [14]. Two common mesoporous structures have been identified within the confines of AAMs: (i) circular hexagonal – where the mesopores wind around the main axis of the AAM channels and (ii) columnar hexagonal – where the mesopores run parallel to the main axis of the AAM channels. Recently another confined mesoporous structure has been postulated, *i.e.* a lamellar structure which is composed of concentric silica sheets [12]. In terms of applications, mesoporous silica filaments in AAMs have been used as templates for the synthesis of carbon filaments [15] and in the controlled delivery of drugs [16, 17].

The analysis of PMO filaments confined with the porous structure of AAMs has also been studied in the past, most recently using small angle x-ray scattering (SAXS) and transmission electron microscopy (TEM) by Keilbach *et al.* [18]. Electrophoretic deposition of PMO materials within AAM channels was investigated by Hill *et al.* [19] and depositions using a PMO gel with two different structural directing agents was reported by Lee *et al.* [20]. Ku *et al.* [21]

and Lai *et al.* [22] both reported the deposition of various mesoporous materials within the channels of AAMs and the growth of nanowires within the pores of mesoporous silica confined within the channels of AAM was reported by Petkov *et al.* [23]. Marlow *et al.* also studied circular mesoporous silica filaments synthesised in the absence of an AAMs using SAXS [24].

In this paper we report the synthesis of PMOs, through a sol-gel process, within the pores of AAMs. The effects of the deposition conditions, *e.g.* reduced humidity as well as the organic – inorganic ratio, on the resultant porous structure were investigated to enable a detailed understanding of the dynamics of the disorder-to-order transitions in these systems and to subsequently control the orientation of the mesostructured phases.

Experimental

P123 was supplied by BASF. Tetraethyl orthosilicate (TEOS), 2-bis-(triethoxysilyl) ethane (BTESE) were supplied by Sigma-Aldrich. All chemicals were used as received. Ethylene-bridged PMO materials within the AAMs were prepared from a sol-gel method similar to that reported previously by Platschek *et al*. [25]. In a typical synthesis 2.08 g w/w of silica (TEOS) and organo-silica (BTESE) precursors, 3 ml of 0.2 M aq HCl, 1.8 mL of H_2O and 5 mL of ethanol were mixed at 60 °C for 1 hr. To this solution, 15 mL of a 5 wt % P123 in ethanol was then added and left to stir at room temperature for 1 hr, after which the gel was filtered. The gel was then dropped onto a Whatman AAM, with 100 nm pores, until the membrane was completely covered and left to dry under vacuum or in a controlled humidity atmosphere. Dry AAM-PMO composites where calcined at 450 °C in air to lift off any excess film material from the surfaces of the membrane. It should also be noted that the calcination step also reduces the

size of the PMO filament within the AAM pores and adhesion between the PMO filament and the AAM wall is lost. The SAXS experiments were first conducted *ex-situ* on already structured (dry) membranes followed by *in-situ* time resolved experiments on some selected samples. This however resulted in a mesoporous film deposited on top of the membrane which interfered with, but did not obstruct, the analysis of the mesoporous filaments within the AAM channels. This surface film is unavoidable when conducting *in-situ* measurements, where otherwise it would be removed via calcination or polishing.

Characterisation

In-situ SAXS experiments at grazing incidence angles of 1 to 2 degrees were carried out at the Austrian SAXS beamline of the ELETTRA Synchrotron facility, Trieste, Italy using an image intensified 2D-CCD-camera (CV12, Photonic Science Ltd, Millham, UK) and 8 KeV x-ray energy. The sample to detector distance was set to 1.478 m. Briefly, the AAMs were loaded with the PMO gel in a sealed chamber in which the humidity was controlled. In some cases the evaporation rate was accelerated by evacuating the chamber to a reduced pressure of approximately 1 mbar. D-spacings were calculated using a standard (silver behenate) of known d-spacing.

TEM images were collected on a JEOL 2000FX transmission electron microscope operating at a voltage of 200 kV. The membranes were prepared for plan-view TEM imaging by dimple grinding, followed by Ar-ion polishing. The dimple grinding was accomplished using a Gatan model 656 dimple grinder using 5 µm diamond paste. Further Precision Ion Polishing (PIPS)

reduces the thickness of the AAM for TEM analysis which was done at grazing angles of 6° with a 5 kV acceleration voltage on a Gatan, Precision ion polishing system model 691.

Results and Discussion

SAXS measurements of AAMs loaded with a mesoporous material will result in different diffraction patterns due to the orientation of the mesostructure within the AAM channels, see Figure 1. These diffraction patterns are much like those reported for normal mesoporous thin films, as reported by Grosso *et al.* [26, 27]. However due to the confinement effects of the AAM channels different scattering patterns are observed. A very good overview of such x-ray reflections and the responsible structures, in direct space and reciprocal space, are given by Platschek *et al.* [12] and briefly repeated here for completeness.

Figure 1(a) shows the columnar hexagonal mesoporous structure and the scattering pattern which results from the high rotational symmetry of the columnar structure around the axis of the AAM channels. Figure 1(b) illustrates the circular hexagonal mesoporous structure consisting of concentric circles of hexagonally arranged pores wound around the AAM channels and an example of the resulting scattering pattern from the circular hexagonal pores. The additional scattering spots are hidden from view due to the beam stop. Additionally, a lamellar mesophase (concentric lamellar sheets wound around the axis of the AAM channels) has also been reported [12, 25], however such a structure was not observed in this work. SAXS data was not the only technique used to identify the mesoporous structures present in the AAM channels as SAXS data may lead to misleading conclusions. Therefore complementary TEM data was used to confirm the mesoporous structures within the AAM channels.

The evaporation induced self assembly (EISA) mechanism that determines the final structure of a PMO materials can be influenced by many factors [26], none more important than the chemical composition of the deposited gel [28]. Humidity play a significant role during the condensation of a silica precursor during the deposition of any mesoporous material. Water is vital to both the condensation of the silica precursor and the formation of stable micelles of the structure directing agent (in this case P123). The effect of humidity on the final mesoporous structure within the AAM channels from a sol composed of 50 % w/w organosilica precursor and 50 % w/w silica precursor measured *ex-situ* is shown in Figure 2.

The presence of the (10) and (01) scattering spots shown in Figure 2(a) indicate both in-plane and out-of-plane scattering resulting from circular hexagonal mesopores within the AAM channels. In contrast, samples deposited at reduced humidity show scattering patterns where only the in-plane reflections are present (Figures 2(b) and 2(c)) which results from the mesopores ordered in a columnar hexagonal fashion. As explained previously, in order to uniquely identify these structures as columnar, complementary TEM data is required. Figure 3 shows plan-view TEM images for two samples deposited at high and low humidity from the same synthetic mixture containing 50 % organosilica and 50 % silica precursor in the deposited gel. The appearance of a lamellar phase in Figure 3(b) cannot be entirely ruled out. The TEM images clearly show that the sample deposited at high humidity is primarily circular phase whereas the sample prepared at reduced humidity has largely columnar pores. In both cases a partial mixture of phases exists. In Figure 3(a) it can be seen that the ordering of the hexagonal columnar phase

is very well structured at the extremities of the mesoporous filament, which has been proposed to result from increased micelle ordering near the AAM channel walls [22].

A gel used to deposit mesoporous thin films similar to the one used in this work can be described as a pseudo liquid crystal, which depending on the rate of evaporation of ethanol and water, and the resulting concentration of the structure directing agent (SDA), determines the structure of the final mesophase formed [29]. The rate of condensation of the mesoporous framework is constant at any given humidity, however when the mesoporous framework is no longer flexible enough to adapt to the changing micelle shape after prolonged condensation for example, the resulting mesophase is determined. During this study the gel deposition at higher humidity results in the slower evaporation of both ethanol and water, due to the diffusion of water from the surrounding atmosphere into the thin film gel, resulting in circular hexagonal ordered mesopores. The circular structure is suggested from the SAXS pattern shown Figure 2(a). In a less humid atmosphere ethanol and water evaporate much faster resulting in columnar mesoporous, as seen in the SAXS patterns shown in Figures 2(b) and 2(c).

During the evolution of mesoporous materials the volatile components in the sol-gel evaporate over time which leads to a surfactant and silica precursor rich gel. At the same time the acidic component of the gel initiates the condensation of the silica precursor. As both these processes progress the mesoporous network experiences a contraction in the porous structure during synthesis. This contraction is continued if the mesoporous material is further calcined at any temperature. In a thin film the contraction is perpendicular to the surface of the substrate [30] and has been known in some cases to contribute to changes in the pore morphology [31]. This

contraction is also experienced by the mesoporous filaments within the AAMs and results in the contact failure between the mesoporous filaments and the AAM pore walls. When the mesoporous gel dries in a low humidity atmosphere the volatile components (ethanol, water and HCl) evaporate at a much faster rate, compared to drying in a high humidity atmosphere, and the PMO network experiences different contraction stresses. These different contraction stresses are likely to be responsible for the dissimilar structures produced within the AAMs. There is a d-spacing increase of 20 Å when the organosilica content is increased from 50 to 100 %.

The drying rate and hence the condensation and disorder-to-order transition process is also thought to be influenced by the amount of organosilica precursor in the deposition gel. Figure 4 shows how the SAXS patterns of the composite membranes change when the amount of organic component is changed in the deposition gel. There is a definite change in the mesoporous structure as the organosilica component of the gel is increased from (a) 50 % to (b) 75 % (b) and (c) 100 % at a constant humidity of 20 %. This change in mesophase from a columnar to circular pore structure can be attributed to an increase of the organic component, which affects the normal surfactant-TEOS interactions (see Figure 4(c)). There is also a slight increase in the d-spacing by 20 Å when the amount of organosilica precursor in the gel is increased from 50 to 100 %.

Figures 4(b) and 4(c) also shows scattering from the surface film of the AAM-silica composite. The intense green circled scattering spots are thought to originate from a 2 D hexagonal mesoporous thin film on the surface of the AAMs. The red scattering spots originate from the circular pore structure of mesoporous-AAM filaments. These green circled spots can be indexed

as 2 dimensional hexagonal (01), (10) and (01) from left to right and can be seen to occur at different positions compared to the mesoporous structures formed within the AAM channels. This surface film hinders the mass transfer of the gel within the channels of the AAMs and the presence of this surface film is further verified by time resolved SAXS measurements as discussed below. The intense scattering arc at larger q-values (larger distance from the beam centre) is thought to result from a disordered material also present on the silica-AAM composite surface.

The evolution of the different mesoporous structures as a function of time, at varying deposition conditions and reaction mixtures, was investigated by SAXS. Figures 5 and 6 show time-resolved SAXS measurements conducted on a 50 % w/w organosilica gel, deposited at 20 % relative humidity (Figure 5) and under vacuum (Figure 6). Scattering patterns from the organosilica gel deposited at 20 % relative humidity emerges after approximately 120 seconds (not shown in figure), with the formation of a (0-1) reflection (due to the columnar structure) at a d-spacing of 116 Å (Figure 5). The position of this reflection remains constant until approximately 600 seconds, at which point the columnar structure experiences a slight contraction. The intensity of the (0-1) reflection remains constant from the initial emergence of the structure until the end of the experiment. The variation in the d-spacings seen between the two experiments is thought to be due to a greater extent of drying in the sample aged under vacuum.

Scattering patterns from the organosilica gel deposited under vacuum emerges approximately 8 seconds after the vacuum is applied (not shown in Figure 6). Throughout the duration of the

experiment the d-spacing of the (0-1) reflection (again due to the columnar hexagonal structure) remains constant at 86 Å, with only a drift of 1 or 2 Å during the course of the experiment. The intensity of the (0-1) reflection also remains constant throughout the experiment.

As expected the rate of evolution of the mesoporous structure is dependent on the rate of solvent evaporation, *i.e.* under vacuum the evaporation of the volatile components proceeds almost instantaneously, seemingly within the first 8 seconds (Figure 6). However, it takes more than 2 minutes for the structure to evolve when the sol gel is left to dry in reduced humidity conditions (Figure 5). In both cases, in the early stages of the deposition process isotropic scattering from the surface 2D hexagonal over-layer is observed before the disorder-to-order transition in the AAM channels is detected. The isotropic ring suggests that the deposited gel solution contains micelles of similar sizes but lacks order in both direction and orientation. Generally in both cases the expected columnar structure is obtained however careful examination of the scattering pattern sequences show that the mesoporous structures are evolving differently as time progresses (see the bottom half of Figure 6 which illustrates the experiment in greater detail). For example, after approximately 300 seconds for the sample shown in Figure 5 the mesoporous ordering is observed on the membrane surface (indicated by the arrow in the 330s frame) due to the accelerated evaporation of ethanol from the surface over-layer gel. The columnar mesoporous structure within the AAM channels starts to appear at approximately 460 seconds (indicated by the arrow in the 465s frame) while scattering from the ordered region of the mesophase surface starts to disappear. After 600 seconds the structure of the mesoporous filaments remains constant with a slight contraction due to continued drying and condensation of the mesoporous framework. Evolution of the mesoporous structure under vacuum (Figure 6)

shows the diffuse scattering ring has the same d-spacing as the ordered columnar structure observed within the AAM channels. The transformation from diffuse scattering to ordered structure within the AAMs is very fast, occurring at about 50 seconds after the start of the deposition. Interestingly, an additional scattering spot at a higher q-parameter (scattering parameter) appears in the in-plane direction at approximately 45 seconds and stays intact until the end of the experiment. This scattering may be attributed to the appearance of a lamellar phase along with the columnar hexagonal phase already thought to be present in the AAM channels. The bottom half of Figure 6 shows a more detailed view of the experiment. Hence the fast drying rate induces the quick concentration of non-volatile gel components (silica and organosilica precursors and non-ionic surfactant) which causes formation of the columnar hexagonal phase.

The structures obtained under accelerated drying rates are remarkably different from those structures obtained at the reduced humidity conditions, where normally a single phase material is obtained by slowly reaching the disorder-to-order transition.

Conclusions

We have shown that mesoporous silica filaments with a PMO component can be obtained within the channels of AAMs. Additionally, we illustrate the resulting mesoporous structures within the pores of the AAM when the deposition environment is controlled. Depending on the rate of evaporation of the volatile components in the deposition gel and the contraction stresses experienced by the condensing mesostructure, different mesoporous arrangements can be formed. Time resolved measurements showed the evolution of different structures as the silica-

AAM composite membranes developed in reduced humidity conditions and under accelerated vacuum drying. This work highlights the importance of the environment on the synthesis of mesoporous materials and the control needed to produce the desired material morphology.

Acknowledgements

The authors acknowledge financial support from the Centre for Research on Adaptive Nanostructures and Nanodevices (CRANN) (Project PR22) and from the European Community through its Access to Research Infrastructure action of the Improving Human Potential Programme. This research was also enabled by the Higher Education Authority Program for Research in Third Level Institutions (2007-2011) via the INSPIRE programme.

References

[1] B. J. Melde, B. T. Holland, C. F. Blanford and A. Stein, Chem. Mater. 11 (1999) 3302-3308.

[2] S. Inagaki, S. Guan, Y. Fukushima, T. Ohsuna and O. Terasaki, J. Am.Chem. Soc. 121 (1999) 9611-9614.

[3] B. Hatton, K. Landskron, W. Whitnall, D. Perovic and G. A. Ozin, Acc. Chem. Res. 38 (2005) 305-312.

[4] Q. H. Yang, J. Liu, L. Zhang and C. Li, J. Mater. Chem. 19 (2009) 1945-1955.

[5] S. Shylesh, P. P. Samuel, S. Sisodiya and A. P. Singh, Catalysis Surveys from Asia 12 (2008) 266-282.

[6] Y. Yang and A. Sayari, Chem. Mater. 19 (2007) 4117-+.

[7] V. Rebbin, M. Jakubowski, S. Potz and M. Froba, Microporous Mesoporous Mater. 72 (2004) 99-104.

[8] K. Landskron, B. D. Hatton, D. D. Perovic and G. A. Ozin, Science 302 (2003) 266-269.

[9] A. P. Wight and M. E. Davis, Chem. Rev. 102 (2002) 3589-3613.

[10] F. Hoffmann, M. Cornelius, J. Morell and M. Froba, J. Nanosci. Nanotechnol. 6 (2006) 265-288.

[11] S. Y. Wu, H. S. Hsueh and M. H. Huang, Chem. Mater. 19 (2007) 5986-5990.

[12] B. Platschek, R. Kohn, M. Doblinger and T. Bein, Langmuir 24 (2008) 5018-5023.

[13] B. Platschek, R. Kohn, M. Doblinger and T. Bein, Chemphyschem 9 (2008) 2059-2067.

[14] Q. S. Huo, D. Y. Zhao, J. L. Feng, K. Weston, S. K. Buratto, G. D. Stucky, S. Schacht and F. Schuth, Adv. Mater. 9 (1997) 974-&.

[15] D. J. Cott, N. Petkov, M. A. Morris, B. Platschek, T. Bein and J. D. Holmes, J. Am. Chem. Soc. 128 (2006) 3920-3921.

[16] V. Cauda, L. Muhlstein, B. Onida and T. Bein, Microporous Mesoporous Mater. 118 (2009) 435-442.

[17] V. Cauda, B. Onida, B. Platschek, L. Muhlstein and T. Bein, J. Mater. Chem. 18 (2008) 5888-5899.

[18] A. Keilbach, M. Doblinger, R. Kohn, H. Amenitsch and T. Bein, Chem.-Eur. J. 15 (2009) 6645-6650.

[19] J. J. Hill, S. P. Cotton and K. J. Ziegler, Chem. Mater. 21 (2009) 1841-1846.

[20] K. J. Lee, S. H. Min and J. Jang, Chem.--Eur. J. 15 (2009) 2491-2495.

[21] A. Y. Ku, S. T. Taylor, W. J. Heward, L. Denault and S. M. Loureiro, Microporous Mesoporous Mater. 88 (2006) 214-219.

[22] P. Lai, M. Z. Hu, D. Shi and D. Blom, Chem. Comm. (2008) 1338-1340.

[23] N. Petkov, B. Platschek, M. A. Morris, J. D. Holmes and T. Bein, Chem. Mater. 19 (2007) 1376-1381.

[24] F. Marlow, I. Leike, C. Weidenthaler, C. W. Lehmann and U. Wilczok, Adv. Mater. 13 (2001) 307-310.

[25] B. Platschek, N. Petkov and T. Bein, Angew. Chem., Int. Ed. 45 (2006) 1134-1138.

[26] D. Grosso, F. Babonneau, P. A. Albouy, H. Amenitsch, A. R. Balkenende, A. Brunet-Bruneau and J. Rivory, Chem. Mater. 14 (2002) 931-939.

[27] D. Grosso, F. Babonneau, C. Sanchez, G. J. D. A. Soler-Illia, E. L. Crepaldi, P. A. Albouy, H. Amenitsch, A. R. Balkenende and A. Brunet-Bruneau, J. Sol-Gel Sci. Technol. 26 (2003) 561-565.

[28] C. J. Brinker, Y. F. Lu, A. Sellinger and H. Y. Fan, Adv. Mater. 11 (1999) 579-+.

[29] F. Cagnol, D. Grosso, G. J. D. A. S. Soler-Illia, E. L. Crepaldi, F. Babonneau, H. Amenitsch and C. Sanchez, J. Mater. Chem. 13 (2003) 61-66.

[30] M. P. Tate, B. W. Eggiman, J. D. Kowalski and H. W. Hillhouse, Langmuir 21 (2005) 10112-10118.

[31] E. L. Crepaldi, G. J. D. A. Soler-Illia, D. Grosso, F. Cagnol, F. Ribot and C. Sanchez, J. Am. Chem. Soc. 125 (2003) 9770-9786.

Figure Captions

Figure 1. Schematics of the mesoporous structures within the channels of AAMs with the corresponding SAXS patterns: (a) columnar hexagonal, (b) circular hexagonal orientated mesoporous structure.

Figure 2. The influence of the humidity during the deposition of the mesoporous material from a sol composed of 50 % w/w organosilica precursor and 50 % w/w silica precursor measured: (a) high humidity (80 %), (b) moderate humidity (40 %) and (c) low humidity (20 %).

Figure 3. Plan view TEM images of mesoporous structures deposited from a gel containing 50 % organosilica precursor and 50% silica precursor deposited at (a) 20 % and (b) 80 % relative humidity. Scale bar corresponds to 100 nm.

Figure 4 SAXS patterns of mesoporous structures deposited at 20 % relative humidity from gels containing (a) 50 %, (b) 75 % and (c) 100 % w/w organosilica precursor. The circled regions in Figure 4 (b) and (c) are explained in the text.

Figure 5 Time resolved SAXS patterns of mesoporous structure deposited from a gel containing 50 % organosilica precursor at a relative humidity of 20 %. The gel was dropped nto the surface of the membrane, positioned in a humidity chamber and the relative humidity was set to 20 %. The measurements started 5 min after the sol gel was introduced on the membrane surface.

Figure 6 Time resolved SAXS patterns of mesophase structures deposited from a gel containing 50 % organosilica precursor under vacuum. The sol gel was drop casted on the surface of the membrane, positioned in a vacuum chamber and the vacuum was introduced 15 s

after the start of the measurement. The bottom half of the Figure shows a more detailed view of the time resolved experiment over the same time range.

Figures

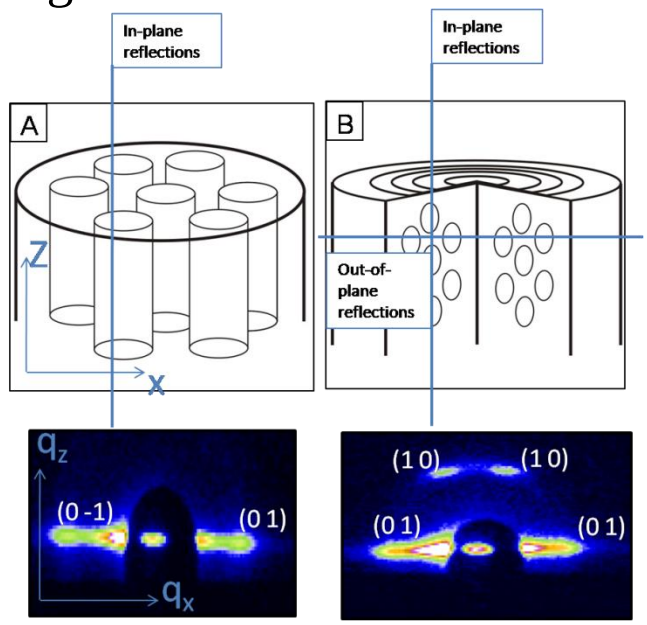

Figure 1

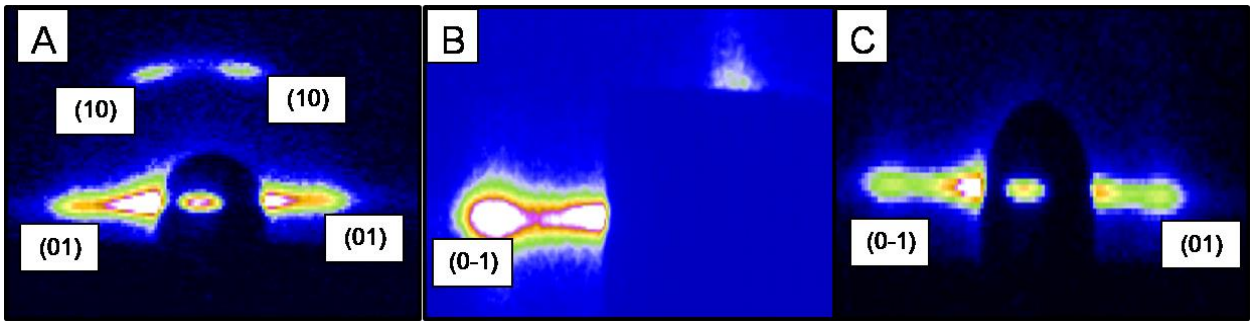

Figure 2

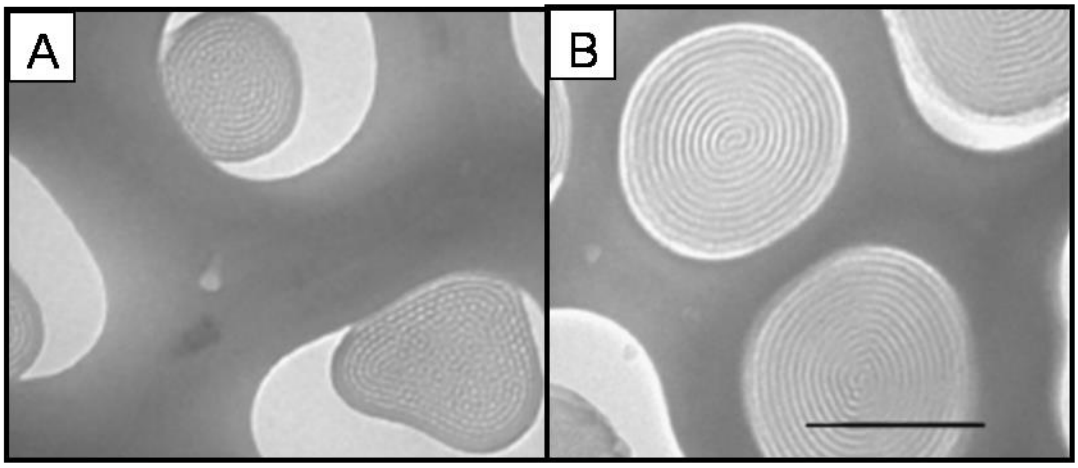

Figure 3

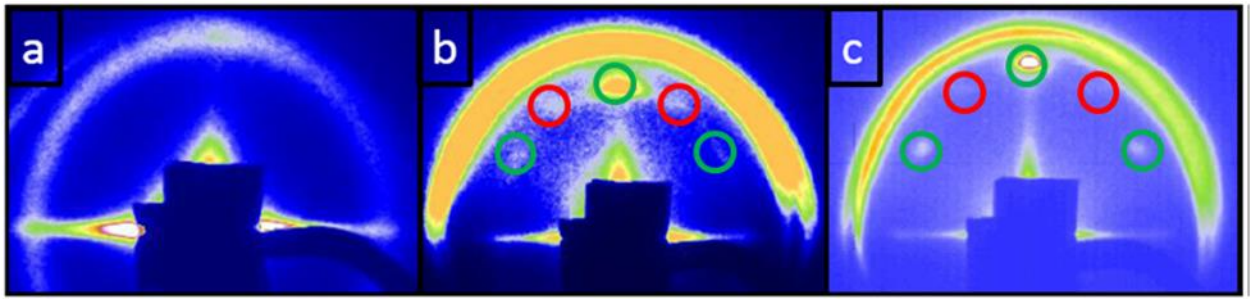

Figure 4

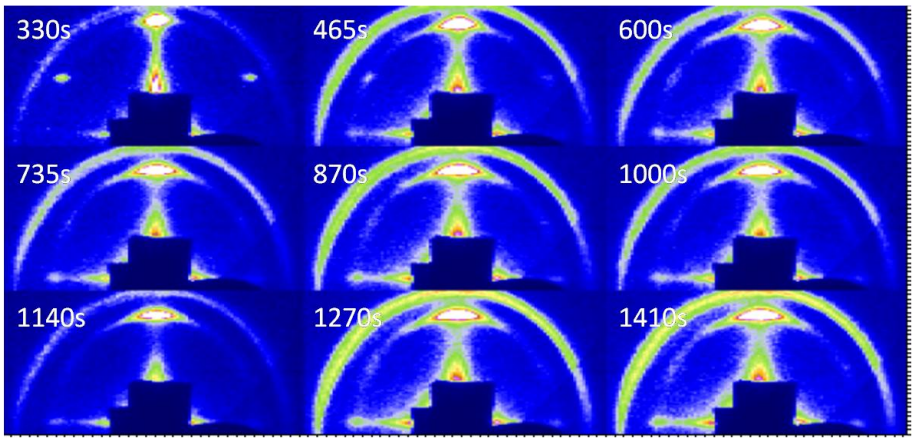

Figure 5

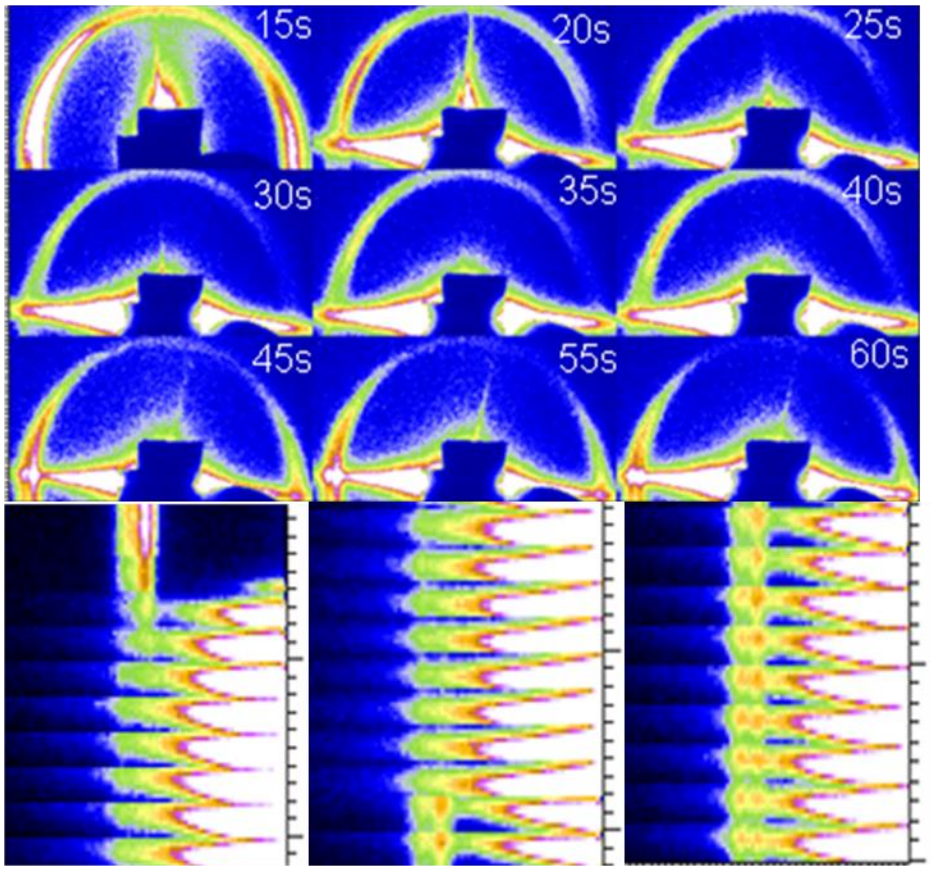

Figure 6